Tuaimenal A, a meroterpene from the Irish deep-sea soft coral *Drifa* sp., displays antiviral and antiproliferative bioactivity.

Nicole E. Avalon,[†] Jordan Nafie,[§] Tracess Smalley,[‡] Carolina De Marco Verissimo,[††] Sarah G. Dietrick,[†] Ryan M. Young,[‡‡] Luke C. Warrensford,[†] Amanda R. Pittman,[†] Fiona L. Kearns,[†] Jennifer M. Binning,[‡] John P. Dalton,[††] Mark P. Johnson,[‡‡] H. Lee Woodcock,[†] A. Louise Allcock,[,‡‡] and Bill J. Baker*[,†]*

Contact information for the Corresponding Authors: louise.allcock@nuigalway.ie (ALA), bjbaker@usf.edu (BJB)

[†]Department of Chemistry, University of South Florida, Tampa, FL, USA. [§]BioTools, Inc., Jupiter, FL, USA. [‡]Department of Molecular Oncology, H. Lee Moffitt Cancer Center and Research Institute; Tampa, FL, USA. [††]Molecular Parasitology Laboratory (MPL), Centre for One Health and Ryan Institute, School of Natural Science, National University of Ireland Galway, Galway, Republic of Ireland. [‡‡]School of Natural Sciences and Ryan Institute, National University of Ireland Galway, H91 TK33 Galway, Republic of Ireland.

KEYWORDS: Terpene, Cnidarian, Vibrational Circular Dichroism, SARS-CoV-2, Cancer, Flexible Docking, 3CLpro

ABSTRACT

Cold water benthic environments are a prolific source of structurally diverse molecules with a range of bioactivity against human disease. Specimens of a previously chemically unexplored soft coral, *Drifa* sp., were collected during a deep-sea cruise that sampled marine invertebrates along the Irish continental margin in 2018. Tuaimenal A (**1**), a cyclized merosesquiterpenoid representing a new carbon scaffold with a highly substituted chromene core, was discovered through exploration of the soft coral secondary metabolome via NMR-guided fractionation. Absolute stereochemistry was determined through vibrational circular dichroism. Functional assays and *in silico* docking experiments found tuaimenal A active against two major health burdens: SARS-CoV-2 and cancer. Biochemical and cell-based assays established that tuaimenal A effectively and selectively inhibits the viral main protease (3CLpro) and mitigates proliferation of cervical cancer cells lines. Given the need for novel treatment options for both diseases, our data suggest that tuaimenal A and/or its derivates could culminate in the development of a unique and effective drug.

Ninety-five percent of the ocean floor exceeds depths of 1,000 meters where water temperatures are a constant 4 °C.[1] Over half of the 5,100 known coral species are found in the deep sea, where cold water corals create gardens in benthic regions ranging from 200 – 1000 m depth.[1] Utilizing both physiological and biochemical adaptations, cold water corals have adapted to survive in an environment with minimal-to-no light, extremely high pressures, and intense competition for resources. One biochemical adaptation to these conditions is the production of secondary metabolites.[2] These compounds have unusual and diverse structures that confer a competitive advantage to the organisms but, incidentally, also exhibit high rates of affinity to biological targets implicated in human disease.[2] Natural products from the deep sea comprise less than 2% of known natural products; however, the rate of bioactivity from deep-sea compounds is estimated to be as high as 75%.[2]

Across the world's oceans, the phylum Cnidaria is second only to Porifera in the number of new natural products reported annually from invertebrates.[3] Comprising over three thousand species, Octocorallia are a particularly rich source of natural product exploration; roughly 80% of bioactive compounds from corals have been isolated from this subclass.[4] The Nephtheidae family comprises 20 genera and about 500 species, including the genus *Drifa*. Known colloquially as cauliflower corals due to their appearance, *Drifa* species thrive in cold water benthic environments (Figure 1). Corals from the family Nephtheidae are known to produce steroidal and other terpenoid secondary metabolites,[4,5] but the secondary metabolites of *Drifa* have yet to be described.

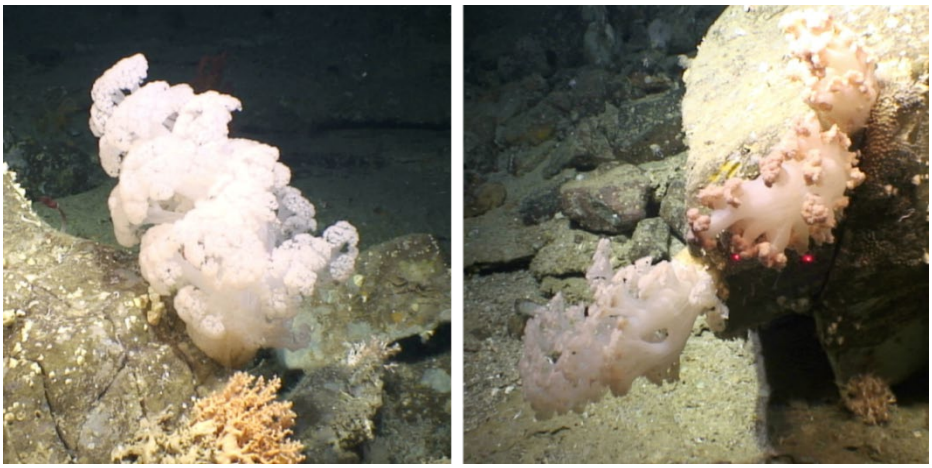

Figure 1. Four specimens of *Drifa* sp. (Cnidaria: Anthozoa: Octocorallia: Alcyonacea: Alcyoniina: Nephtheidae) were collected at a depth of 823 m from a submarine canyon north of Porcupine Bank on the Irish Continental Margin by *ROV Holland I*, deployed from *RV Celtic Explorer*. For scaling a laser light is used (red dots indicate a span of 10 cm). Subsea photographs are copyright Marine Institute, Oranmore, Ireland. Used with permission.

In this study, we sought to analytically characterize and biochemically assess a new natural product from a *Drifa* sp. soft coral. Tuaimenal A (**1**), a compound representing a new carbon scaffold, was discovered through the exploration of the secondary metabolome of the soft coral through NMR-guided fractionation. Paired with high resolution mass spectrometry (HRMS) and NMR for rigorous structure elucidation, vibrational circular dichroism (VCD) was utilized to determine the stereochemistry at the single chiral center. Tuaimenal A is a merosesquiterpene that possesses a highly substituted benzopyran ring system with structural similarity to tocopherol (vitamin E). To assess the bioactivity of this newly identified natural product, we tested its inhibitory properties in a variety of bioassays, including bacterial, fungal and protozoan pathogens. Tuaimenal A demonstrated bioactivity against two major human health burdens: severe acute respiratory syndrome coronavirus 2 (SARS-CoV-2 virus) and cervical cancer.

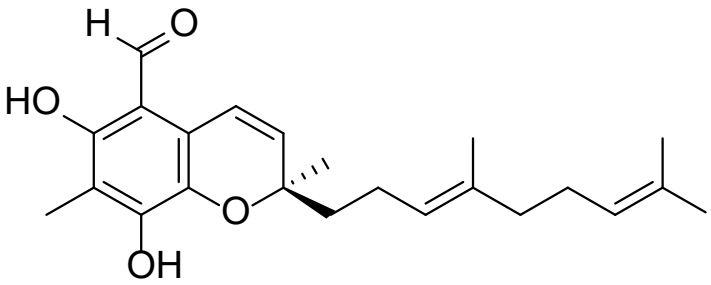

Tuaimenal A (**1**)

The emergence of the SARS-CoV-2 virus from Wuhan, China in late 2019, has led to the rapid spread of the highly infectious and pathogenic virus and subsequent declaration of the COVID-19 pandemic by the World Health Organization on March 11, 2020.[6] The ongoing pandemic caused by this virus is responsible for the deaths of over 2.8 million people worldwide as of the end of 2021.[7] While vaccinations against SARS-CoV-2 are being administered globally, treatment of the disease is limited.

In contrast to the recent emergence of SARS-CoV-2 in the human population, cancer has been a longstanding public health burden and is currently a leading cause of death worldwide.[8,9] While there have been great strides in cancer treatment, there remains overarching challenges such as adaptive drug resistance, relapse, and undesirable side effects (i.e., high toxicity, changes in quality of life). Natural products have played a pivotal role in the development of anti-cancer drugs and chemotherapeutic agents. For instance, 68% of the useful marine natural products have been employed for cancers and between 1981 to 2019, ~ 25% of newly approved anticancer drugs were linked to natural products.[10,11] Therefore, drug discovery and drug repurposing efforts are needed to find effective treatments for both cancer and COVID-19 infections.[12,13]

Herein we report the structure and bioactivity for tuaimenal A (**1**). *In silico* docking identified the major SARS-CoV-2 proteases as targets of tuaimenal A. Biochemical assays established that tuaimenal A selectively inhibits the viral main protease (3CLpro). Cell-based assays further demonstrate that tuaimenal A exhibits anti-proliferation activity in cervical cancer cell lines. In sum, tuaimenal A is a newly discovered natural product with bioactivity that may lead to novel therapeutics against SARS-CoV-2 and cervical cancer.

RESULTS AND DISCUSSION

Structure Analysis of Tuaimenal A (1). Tuaimenal A (**1**)[14] was obtained as a yellow oil with a molecular formula of $C_{23}H_{30}O_4$ based on high-resolution electrospray ionization mass spectrometry (HRESIMS) ($[M + H]^+$ of 371.2216 amu; calculated for $C_{23}H_{31}O_4$ 371.2217, Δmmu 0.1) (Figure S1) and corroborated by NMR data (Table 1, Figure S2, S3). The downfield region of the ^{1}H NMR spectrum (Figure S2), informed by the phase-sensitive gHSQCAD spectrum (Figure S4), revealed several functional groups. The signal at δ_H 12.31 (OH_a) (Figure 2) displayed no HSQC correlation to a carbon, suggesting it was on a heteroatom, and its shift was characteristic of an H-bonded phenol. The shift at δ_H 10.08 (H-11), correlated in the HSQC with δ_C 191.1 (C-11), both of which are consistent with an aldehyde function. A series of olefinic proton shifts from δ_H 5.07 to 6.86, taken with twelve olefinic ^{13}C chemical shifts identified a highly oxidized skeleton; the most deshielded, δ_C 158.2 (C-6) and 151.4 (C-8) are indicative of olefinic/aromatic oxygen-bearing carbons.

Table 1. NMR Spectroscopic Data (400 MHz, $CDCl_3$) for tuaimenal A (**1**)

pos	*δ_C, type*	*δ_H, mult, J (Hz)*	*HMBC*
2	79.1, C		
3	132.4, CH	5.80, d (10.1)	C-2, C-10, C-12′, C-1′
4	116.4, CH	6.86, d (10.1)	C-2, C-3, C-5, C-9, C-10
5	107.5, C		
6	158.2, C		
7	111.7, C		
8	151.4, C		
9	132.3, C		
10	118.7, C		
11	191.1, CH	10.08, s	C-5, C-6, C-7
12	7.6, CH_3	2.14, s	C-6, C-7, C-8
1′	40.2, CH_2	1.78, 2.12, ov[a] m	C-3, C-2′, C-3′
2′	22.6, CH_2	1.76, 2.13, ov m	
3′	123.3, CH	5.11, ov t	C-2′, C-5′, C-11′
4′	135.8, C		
5′	39.6, CH_2	1.99, ov t	C-3′, C-4′, C-6′, C-11′
6′	26.6, CH_2	2.05, ov m	C-4′, C-5′, C-7′, C-8′
7′	124.1, CH	5.07, ov t	C-10′
8′	131.4, C		
9′	25.7, CH_3	1.68, s	C-7′, C-8′, C-10′
10′	17.7, CH_3	1.59, s	C-7′, C-8′, C-9′
11′	16.0, CH_3	1.58, s	C-5′, C-3′, C-4′
12′	25.4, CH_3	1.43, s	C-2, C-3, C-1′
OH_a		12.31, s	C-5, C-6, C-7, C-8
OH_b		6.37, s	C-6, C-7, C-8, C-9

[a]ov: overlapping signals

Further analysis of tuaimenal A (**1**) 2D spectra facilitated the development of additional partial structures. The HSQC was used to assign the remainder of the protons to their respective carbons (Table 1). Taken with the COSY spectrum (Figure S5), spin-coupled systems included vinylic proton δ_H 6.86 (H-4), which shared a COSY correlation with vinylic proton δ_H 5.80 (H-3). The singlet vinyl proton δ_H 5.11 (H-3′) shared a correlation with the 3H singlet at δ_H 1.58 (H_3-11′). Additionally, δ_H 1.68 (H_3-9′) showed correlation to δ_H 5.07 (H-7′) and 1.59 (H_3-10′), resulting in a vinyl gem-dimethyl group terminating a trisubstituted olefin (Figure 2).

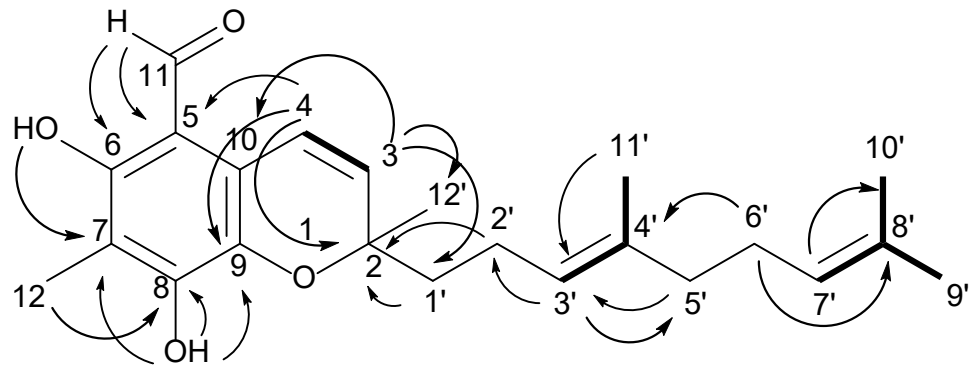

Figure 2. Proposed planar structure of tuaimenal A (**1**) based on NMR data. Key HMBC (→) and COSY (bold bonds) correlations are shown.

HMBC data (Figure S5) were used to extend the partial structures. The signal at δ_H 10.08 (H-11) had multiple correlations, including δ_C 107.5 (C-5), 158.2 (C-6), and 111.7 (C-7), while δ_H 2.14 (H_3-12) shared correlations with C-6, C-7, and δ_C 151.4 (C-8), forming a conjugated system consisting of two olefins and the aldehyde carbonyl (Figure 2). A proton at δ_H 5.80 (H-3) displayed HMBC correlations to δ_C 79.1 (C-2), 118.7 (C-10), 25.4 (C-12′), and 40.2 (C-1′). Similarly, H-4 displayed HMBC correlation to C-2, δ_C 107.5 (C-5), and 132.3 (C-9). Olefinic C-9 and C-10, therefore, are in conjugation with δ_C 116.4 (C-4) and 132.4 (C-3). A singlet proton at δ_H 6.37 (OH_b) had correlation to C-8 and C-9 which, taken with the HMBC correlation between H-4 and C-5, establishes an aromatic ring. The C-2 shift is consistent with carbon bearing oxygen; this quaternary carbon had correlations from H-3, H_3-12′ and δ_H 1.78 (H_a-1′).

Two partial structures established by COSY (*vide supra*) remained to be incorporated in the growing tuaimenal A (**1**) scaffold. While H_2-1′ (δ_H 1.78, 2.12) and H_2-2′ (δ_H 1.76, 2.13) were heavily overlapped, an HMBC correlation between those shifts and δ_C 79.1 (C-2) extended the scaffold. The partial structure from COSY that included δ_H 5.11 (H-3′) and 1.58 (H_3-11′) could be connected to C-2′ based on an HMBC correlation between H-3′ and C-2′. The final intervention of

two methylene groups δ_C 39.6 (C-5′) and 26.6 (C-6′) and the terminal trisubstituted olefin was established by HMBC correlations between δ_H 1.99 (H-5′) and δ_C 123.3 (C-3′); δ_H 2.05 (H-6′) and δ_C 135.8 (C-4′) and 131.4 (C-8′); and δ_H 5.07 (H-7′) and δ_H 17.7 (C-10′), completing the linear scaffold.

Two valences remained unfilled, and the molecular formula of the established scaffold was missing one oxygen. Establishing a pyran ring between C-9 and C-2 would satisfy these last structural features. The resultant chromene is unusual in its highly substituted aromatic ring, the position of carbon branches on the aromatic ring, and the level of oxidation on the aromatic ring.

Stereochemical Evaluation of Tuaimenal A (1). Determination of the absolute configuration of tuaimenal A (**1**) was achieved using vibrational circular dichroism (VCD), a method which can be employed directly on chiral molecules in solution phase.[15–18] The flexible hydrocarbon tail gave rise to a large number of low energy conformations, which presented a challenge for density-functional theory (DFT) calculations. A truncated version of the molecule was initially studied substituting an ethyl group for the flexible hydrocarbon tail. This had a reduced number of low energy conformers (nine) which were rapidly calculated for comparison to the experimental spectra. While there was some congruence, the overall comparison was not satisfactory. A thorough molecular mechanics search of tuaimenal A yielded over 800 conformers in a 5 Kcal/mol range. Using a small Linux cluster with 64 available cores, DFT calculations were performed on all of the conformers at the B3LYP/6-31G(d) level.[19] After removing duplicates and higher energy structures, the resulting 338 unique conformers were Boltzmann averaged to produce the final theoretical spectrum (Figure 3). The *R* enantiomer was used for calculation, and a match to the measured spectrum confirmed the stereochemistry of tuaimenal A as *R*. The comparison of experimental and theoretical spectra was quantified[20,21] using BioTools CompareVOA® software,

with high neighborhood similarity for IR (90.6) and VCD (57.5), Enantiometic Similarity Index for VCD (35.6) and a confidence level of 86%. A fairly weak VCD signal gave rise to some noise in the experimental spectra which likely reduced the confidence level slightly. Visual comparison of the data makes clear that the assignment is correct, with 11 of the most intense VCD bands well correlated to the experimental data. Overall, this proved to be an effective method to determine the stereochemistry of tuaimenal A.

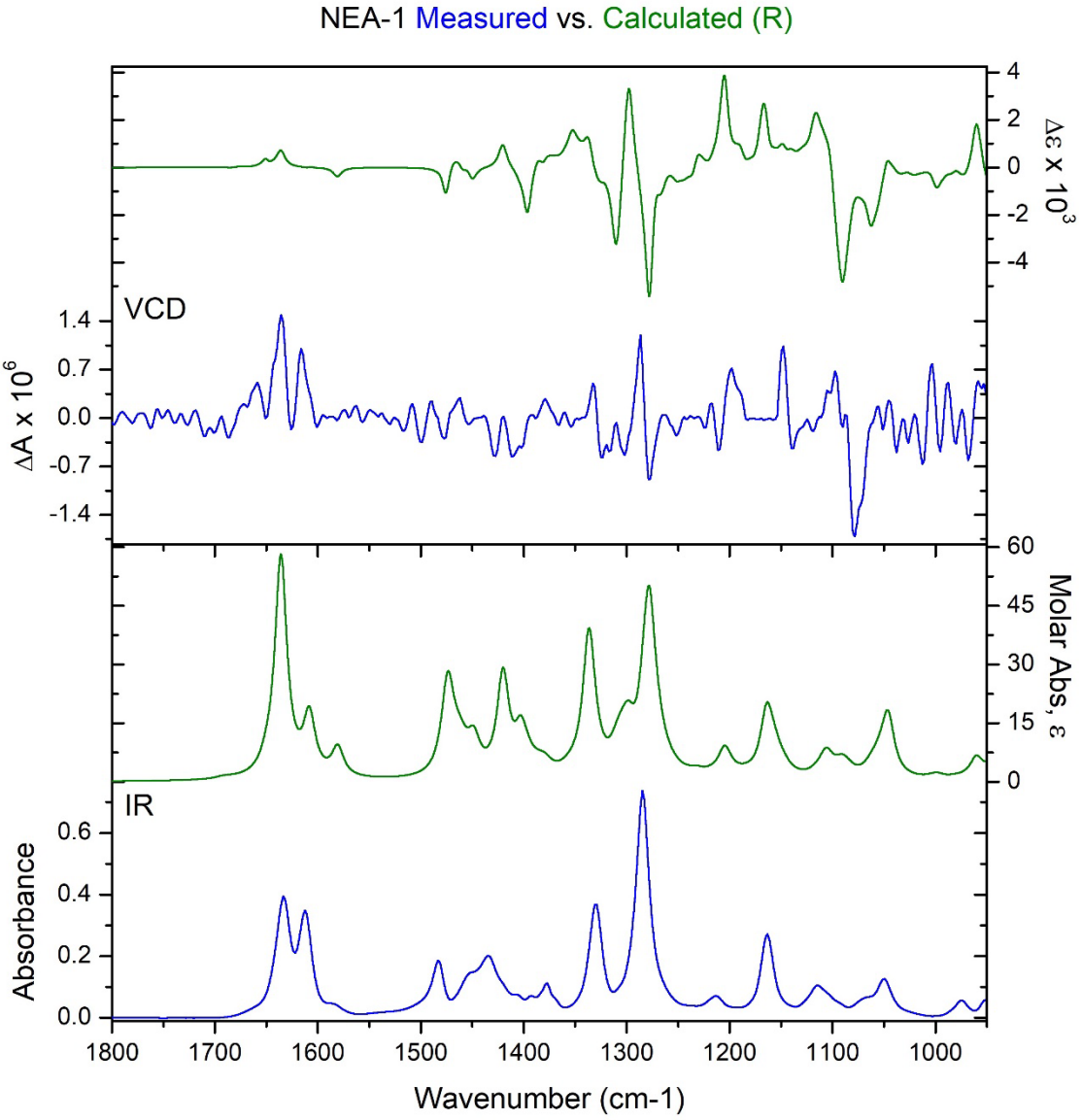

Figure 3. Stereochemistry at C-2 of tuaimenal A (**1**) was determined to be the *R* configuration based on VCD analysis. Top graph shows the congruence between the calculated VCD for the *R* configured stereocenter (green) and the measured VCD (blue). In the lower graph, the calculated FTIR absorbance (green) also demonstrates congruence with the calculated data (blue).

Rigid Docking of Tuaimenal A (1) in SARS-CoV-2 Protein Targets. Four protein targets were selected for *in silico* experiments based on their critical roles in SARS-CoV-2 infections. The main protease, also known as 3CLpro or Mpro, is the viral protease responsible for cleaving twelve non-structural proteins (Nsp4-Nsp16), allowing for viral maturation.[22] Inhibition of this protease prevents viral replication, making it a highly attractive drug target.[23,24] Similarly, the papain-like protease (PLpro) assists with viral replication by cleaving three non-structural proteins (Nsp1-Nsp3).[22] The host Transmembrane Serine Protease 2 (TMPRSS2) assists in the activation and proliferation roles for SARS-CoV-2, and inhibition of this protein can block cell entry.[25] RNA-dependent RNA-polymerase (RdRp) is a critical component for both replication and transcription of this positive-strand RNA virus, and therefore, another important protein to target.[26]

For docking experiments, Schrödinger's Glide XP scoring function was utilized for ranking and analyzing tuaimenal A (**1**) poses. Glide scores are reported for each pose and represent a correlation between the protein-ligand complex and the binding energy.[27] The criterion for selecting favorable poses was a threshold of -7.0 or lower, and ligands are considered to have favorable binding interactions with the target protein when presenting these scores. Validation of binding affinity is observed when multiple ligand conformations are bound to multiple target conformations of the same protein. Tuaimenal A showed a promising profile for binding to both 3CLpro and PLpro (Figure 4). Six favorable poses of tuaimenal A were observed across three of

the 3CLpro structures (i.e., three different protein conformations of 3CLpro out of the five total initial receptors, see Methods), of which the lowest Glide score was -8.925, with an average score of -8.165. The favorable binding is attributed to both hydrogen bonding (dashed yellow lines) and pi-pi-stacking interactions (dashed blue lines) with His41 (Figure 5). Eleven favorable poses resulted for three of the PLpro conformations (lowest Glide score of -8.533, average -7.585). Seven favorable poses resulted for three human TMPRSS2 structures (lowest Glide score of -8.282, average -7.750). Only one conformation of tuaimenal A bound favorably to the viral RdRp structure (Glide score of -7.419). Low binding potentials are likely attributed to the fact that RdRp is generally inhibited through covalent rather than intermolecular interactions.[26]

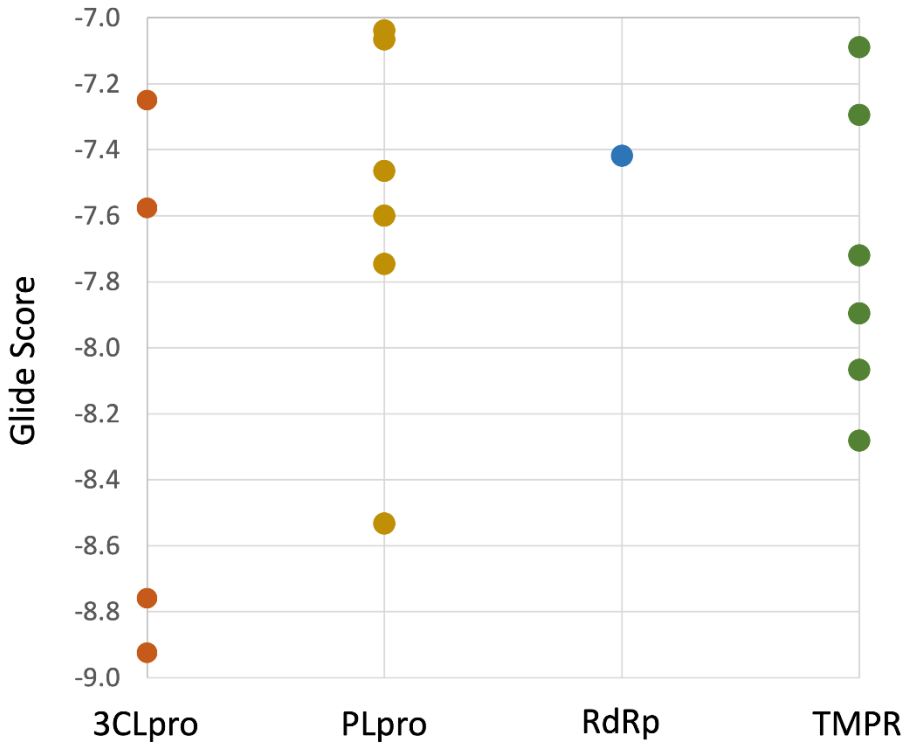

Figure 4. Glide scores for SARS-CoV-2 protein targets for the ligand conformations of tuaimenal A (**1**).

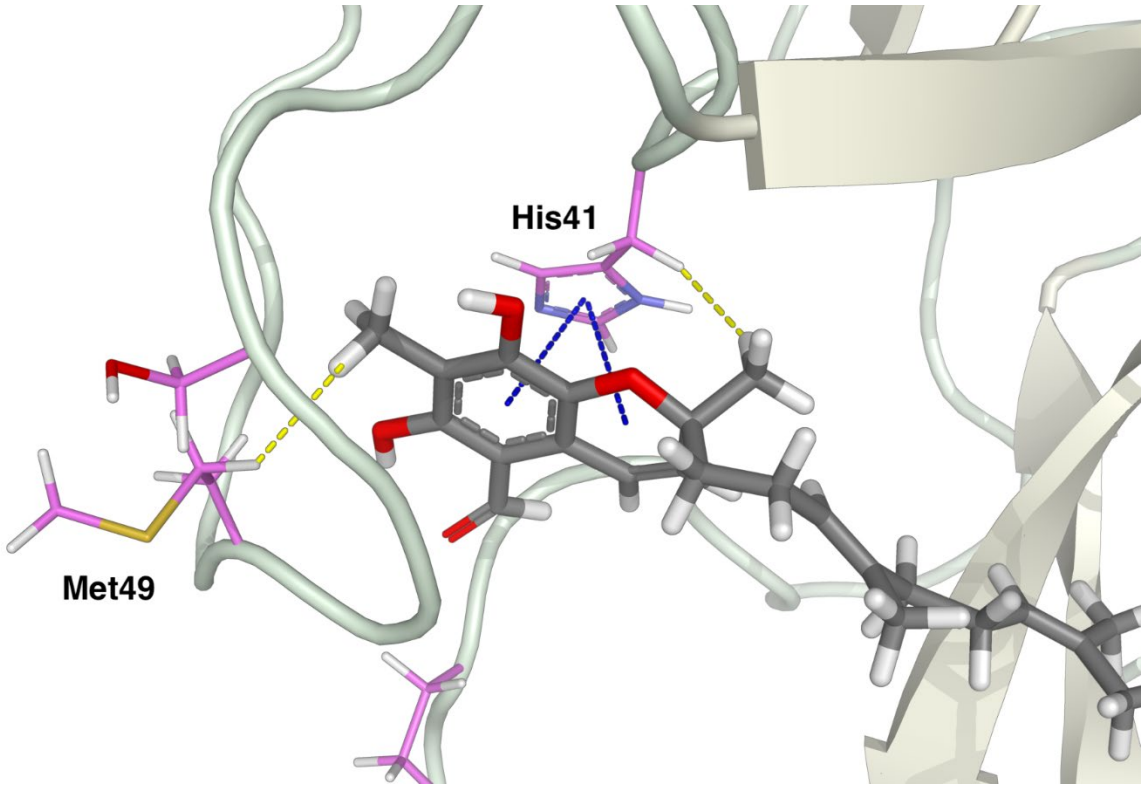

Figure 5. Final pose of tuaimenal A (**1**) Glide docking with 3CLpro, highlighting the two pi-pi stacking interactions (in dashed blue lines) with His41, and hydrogen bonds (in dashed yellow lines) with His41 and Met49.

Flexible Docking of Tuaimenal A (1) in SARS-CoV-2 Protein Targets. A novel CHARMM-based flexible docking protocol, CIFDock,[28] was employed to dock tuaimenal A (**1**) into the same four protein targets (3CLpro, PLpro, RdRp, and human TMPRSS2). This method allows full flexibility of the target receptor and ligand, providing a more thorough conformational space search of tuaimenal A in the active sites of these targets. Rigid docking of tuaimenal A suggested 3CLpro was the most promising of the protein targets. After using CIFDock to flexibly dock tuaimenal A into these proteins, final generated poses were assigned a Glide score using the Glide XP scoring function. The average Glide scores for each tuaimenal A pose in 3CLpro was -10.77

with a lowest scoring pose of -12.42. Docking tuaimenal A with the remaining three proteins, PLpro, RdRp, and human TMPRSS2, resulted in an average Glide score of -7.14, -7.00, and -7.26, respectively. The results from the flexible docking then suggest that tuaimenal A would bind favorably to 3CLpro and may potentially bind to PLpro, RdRp, and TMPRSS2 (Table 2, Figure S9-S11).

Table 2. Results from the flexible docking of tuaimenal A (**1**) into the four SARS-CoV-2 protein targets. Glide scores are averaged across three protein conformations for 3CLpro and PLpro and two for TMPRSS2 and RdRp.

Protein Target	***Average Score***	***Lowest Score***
3CLpro	-10.77	-12.42
PLpro	-7.14	-8.28
TMPRSS2	-7.26	-8.64
RdRp	-7.00	-7.39

The protease-ligand interactions of the lowest scoring final pose between 3CLpro and tuaimenal A (**1**) were visualized (Figure 6). Multiple hydrogen bonding interactions can be seen due to the many acceptor/donor groups on the tuaimenal A topology. Both hydroxyl groups form hydrogen bonds with the protein: one hydroxyl group with Asn28 and the other with Ser144 and Gly146. The hydrogen bond between tuaimenal A and Gly146 is to a backbone atom and is thus not pictured in Figure 6. The tuaimenal A aldehyde oxygen forms hydrogen bonds with Cys117 and Asn119. Finally, the ring oxygen forms a hydrogen bond with the backbone nitrogen of Cys145. Overall, tuaimenal A forms a network of hydrogen bonds with the 3CLpro that results in an intensely favorable binding with this SARS-CoV-2 protease target.

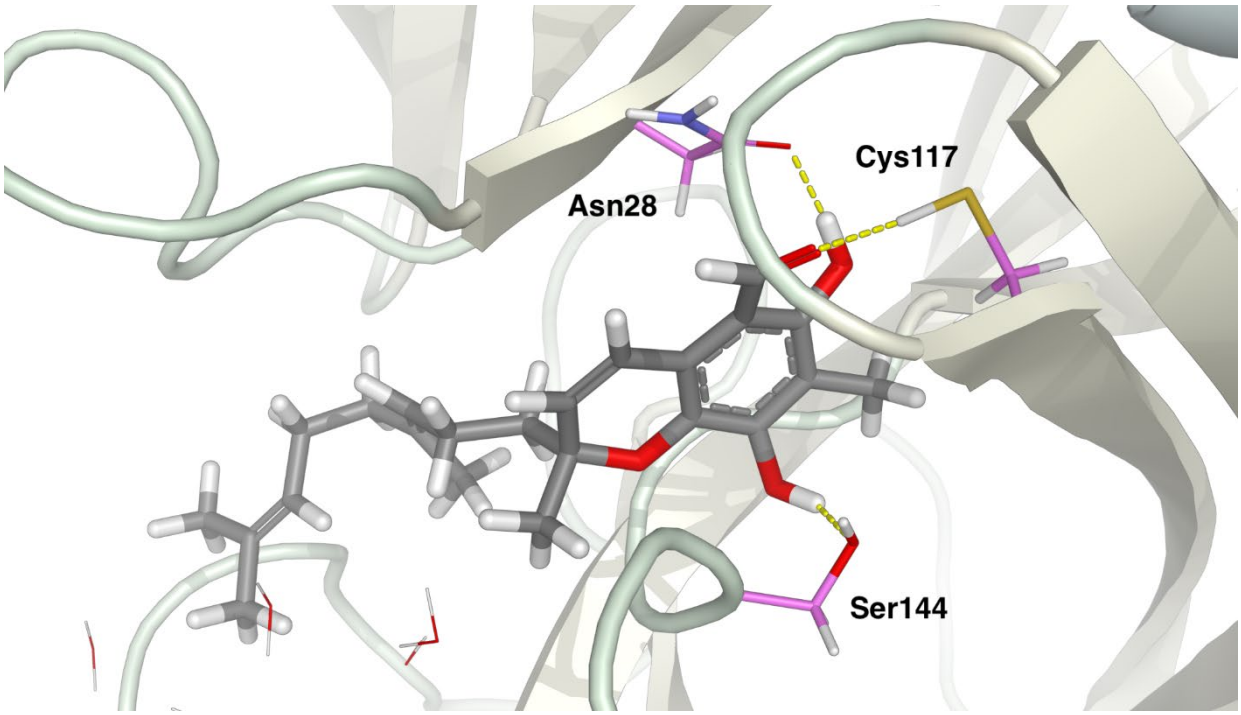

Figure 6. Final pose of the flexible docking of tuaimenal A (**1**) into the main protease (3CLpro). Hydrogen bonds (in dashed yellow lines) can be seen between the ligand and side chains Asn28, Cys117, and Ser144.

Inhibitory Activity of Tuaimenal A (1) Against the 3CLpro. To validate the *in silico* docking experiments, the enzymatic activity of recombinant 3CLpro was measured in the presence or absence of tuaimenal A (**1**). Initially, the compound was screened against the 3CLpro at 20 µM. Tuaimenal A inhibited ~ 40% of the 3CLpro activity, compared to ~100% inhibition obtained with 5 mM AEBSF, a broad-spectrum serine protease inhibitor (Figure 7A). We proceeded to assess the IC_{50} of tuaimenal A against 3CLpro; our data showed that 50% of the activity of the 3CLpro can be abrogated by tuaimenal A at 21µM (Figure 7B). Moreover, further analyses revealed that tuaimenal A behaves as a specific 3CLpro inhibitor as complementary assays with a range of serine and cysteine proteases showed no inhibition when tuaimenal A was used at the same concentration of 20 µM (Figure 7C).

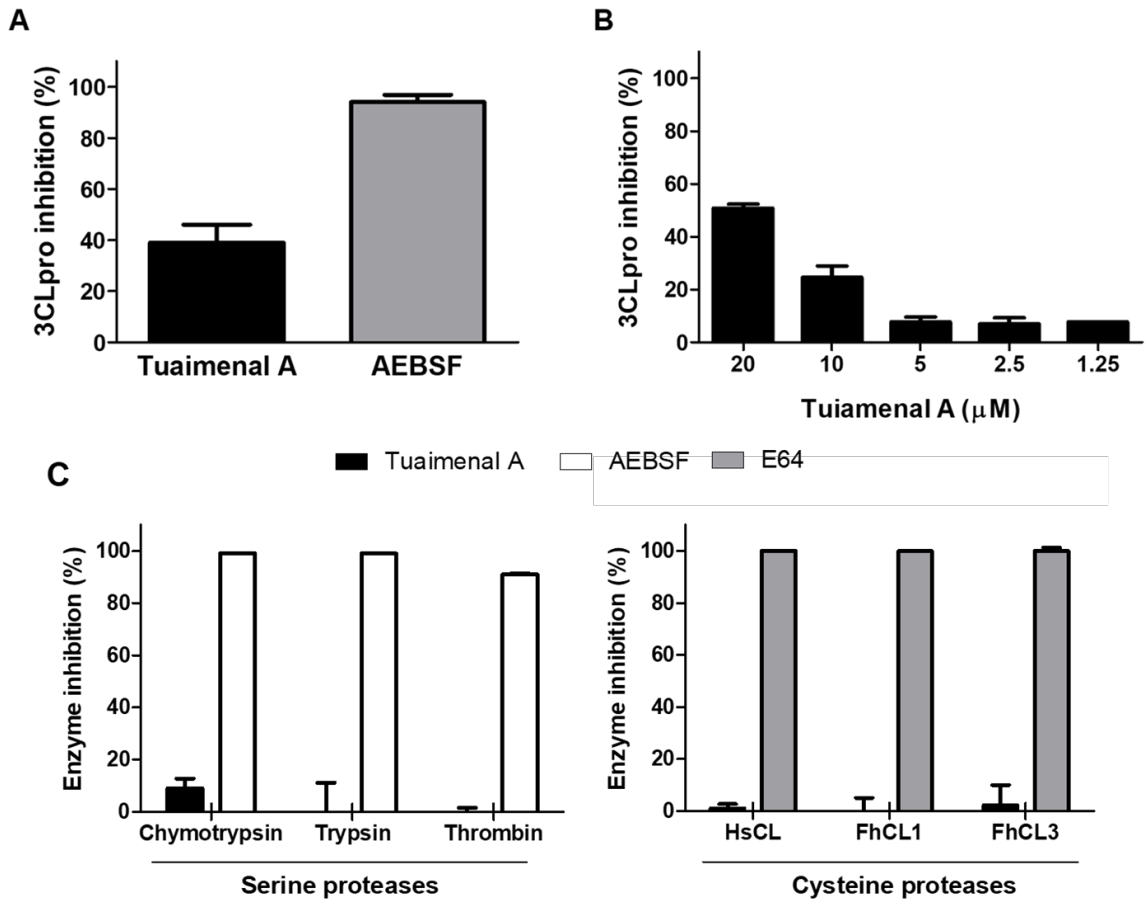

Figure 7 (A&B). Inhibition of 3CLpro activity and evaluation of the specificity of tuaimenal A (1) as a protease inhibitor. (A) The activity of 3CLpro (500 nM) was measured in the presence of tuaimenal A (**1**) (20 μM) or the broad-spectrum serine protease inhibitor, AEBSF (5 mM). (B) Determination of the IC_{50} of tuaimenal A against 3CLpro. The activity of 3CLpro (500 nM) was assayed in the presence of a range of tuaimenal A concentrations (1.25 to 20 μM). Inhibition is presented relative to the activity of 3CLpro in the absence of inhibitors and error bars indicate standard deviation of three separate experiments. (C) The ability of tuaimenal A to inhibit different proteases was evaluated using a panel of serine and cysteine proteases. The activity of the human proteases, chymotrypsin (4.0 nM), trypsin (168 nM), thrombin (800 pM) and HsCL (0.2 nM), or of the unrelated parasite proteases FhCL1 (2.7 nM) and FhCL3 (5 nM), were tested in the presence of 20 μM tuaimenal A (dark bars). The broad-spectrum serine proteases inhibitor AEBSF (5 mM; white bars) or cysteine proteases inhibitor E64 (100 μM, grey bars) was used as a positive

control. Inhibition is presented relative to the activity of each enzyme in the absence of inhibitors and error bars indicate standard deviation of three separate experiments.

Bioassays for Activity Against Cervical Cancer Cell Lines. To evaluate the bioactivity of tuaimenal A (**1**) in cervical cancer models, CaSki, and C33A were employed. Cells were treated with different concentrations (10 μM, 1 μM, 0.1 μM and 0.01 μM) of tuaimenal A and observed using water-soluble tetrazolium salt (WST). After 2 hrs incubation, the cells were evaluated and data revealed that 10 μM of tuaimenal A significantly decreased the proliferation of CaSki cells by >50% and C33A by >40% (CaSki, N=6, *p* value <0.0001, F= 16.17; C33A, N=6, *p* value 0.0002, F= 8.674) (Figure 8).

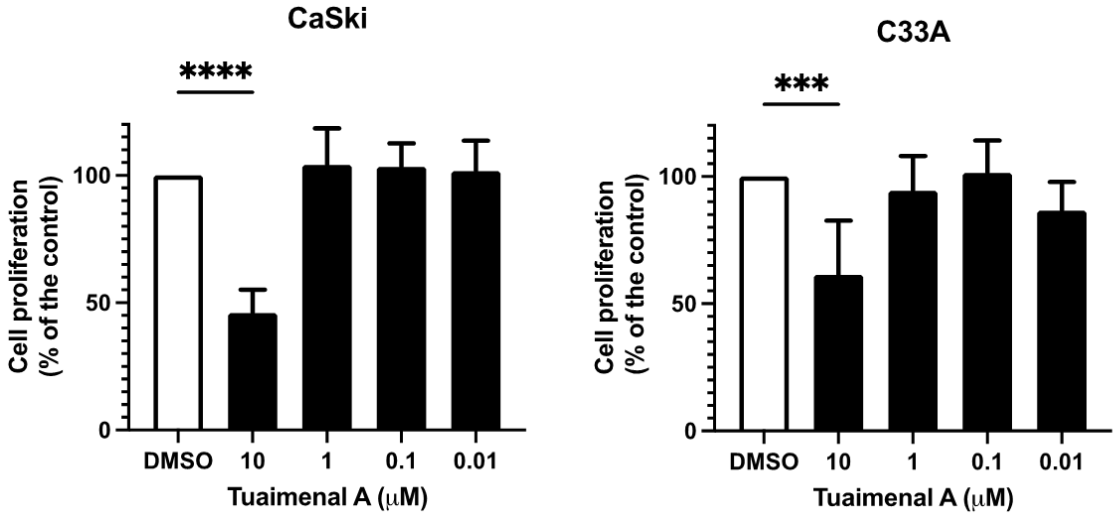

Figure 8. Anti-proliferative effect of tuaimenal A (**1**) on cervical cancer cells. Cervical cancer cells were seeded at 1,000 cells per well in a 96-well plate, grown for 24 hours and were treated with different concentrations (10 μM, 1 μM, 0.1 μM and 0.01 μM) of tuaimenal A. After 24 hours post treatment, the proliferation was observed at wavelengths 450nm and 600nm (reference wavelength) using a BioTek

Synergy HT microplate reader after 2 hours of incubation with WST reagent. Error bars represent standard deviation and significance of a one-way ANONA was $p < 0.0001$ (****) $p < 0.0002$ (***) (N=6).

CONCLUSIONS

Four specimens of the Irish deep-sea coral *Drifa* sp. were explored utilizing NMR-guided fractionation methods. The chemistry of the family Nephtheidae to which it belongs, has been previously described; however, this is the first analysis of the genus *Drifa*. A new natural product, tuaimenal A (**1**), was discovered. This meroterpene represents a new carbon scaffold, a highly substituted merosesquiterpenoid chromene. The benzopyran ring system includes an aldehyde, two phenol features, and a methyl group.

Tuaimenal A (**1**) inhibits the main protease for SARS-CoV-2. *In silico* docking experiments identified 3CLpro as a highly favorable target for tuaimenal A (**1**). Biochemical studies further confirmed that tuaimenal A effectively and selectively inhibits the main protease of SARS-CoV-2. Interestingly, several natural products from terrestrial sources that share a chromene core demonstrate antiviral activity ascribed to 3CLpro inhibition.[29–32] Many drug discovery campaigns have sought to identify inhibitors against the main protease of both SARS-CoV and SARS-CoV-2, highlighting it as a prime antiviral target. Though previous inhibitors have been described, most have been unsuccessful in making their way to the clinic.[32–34] Recently, Pfizer's COVID-19 oral antiviral drug targeting 3CLpro, Paxlovid, was shown to reduce the risk of hospitalization or death by 89% and has received Emergency Use Authorization by the US Food and Drug Administration.[35,36] Despite this success, we still have a very limited number of drugs to treat COVID-19, including remdesivir and monoclonal antibody therapies. To ensure we are well prepared for new variants of concern, especially those that may confer resistance to current

prophylactic or therapeutic treatment options, we need to develop new therapeutics to treat COVID-19 infections. The discovery of tuaimenal A as an inhibitor of SARS-CoV-2 3CLpro suggests that further *in vitro* and *in vivo* studies with this compound and/or derivates of it could culminate in the development of a novel COVID-19 drug.

Natural products have demonstrated efficacy as chemotherapeutic agents for many cancers, including cervical cancer.[37] According to current literature, a total of 64 natural products have been shown to suppress cervical cancer cell lines through mechanisms such as induction of apoptosis, inhibition of angiogenesis, inhibition of metastasis, regulation of miRNAs, and reduction of resistance.[38] Here we show that tuaimenal A (**1**) has an antiproliferative effect in cervical cancer cells models. The mechanistic basis for these anti-proliferative properties is unknown; however, protease inhibitors have been well documented for their use as anti-cancer agents.[39] This investigation warrants further research of the anti-proliferative effects of tuaimenal A as a treatment for cervical cancer in addition to its potential as a complementary therapy to FDA-approved treatments. The discovery of tuaimenal A points to the importance of chemical explorations of deep-sea organisms. Careful sampling and analysis in cold water coral systems can promote drug discovery efforts and underscore the importance of conserving of these natural resources.

MATERIALS AND METHODS

General Procedures. Commercial silica gel 230-400 mesh was used to load samples for MPLC. MPLC was performed on a Teledyne Isco CombiFlash Rf200i with UV detection and a RediSep RF silica flash column. Semipreparative normal phase HPLC was performed on a Shimadzu LC-20 AT system with evaporative light scattering detector (ELSD) and UV detection

using semipreparative (Phenomenex Luna Silica; 250 x 10 mm, 5 μm) or analytical (Phenomenex Luna C18; 250 x 4.6 mm, 5 μm) conditions. Semipreparative non-aqueous reverse phase was performed on a Shimadzu LC20-AT system with a photodiode array detector using semipreparative (Phenomenex Luna C18; 250 x 10 mm, 5 μm) conditions. All solvents were HPLC grade (>99% purity) unless stated otherwise and were obtained from Fisher Scientific. All ^{1}H NMR spectra were recorded at 298K on a Bruker Neo 400 MHz or on a Varian 500 MHz Direct Drive instrument with direct detection, and ^{13}C NMR spectra were recorded at 100 or 125 MHz, respectively. Chemical shifts are reported with the residual chloroform (δ_H 7.27 ppm; δ_C 77.0 ppm) and methanol (δ_H 3.31 ppm; δ_C 49.1 ppm) signals as internal standards for ^{1}H and ^{13}C spectra. IR spectrum was recorded with an Agilent Cary 630 FTIR spectrometer and a PerkinElmer Spectrum Two equipped with a UATR (single reflection diamond) sample introduction system. UV absorptions were measured using an Agilent Cary 60 UV-Vis spectrophotometer. Optical rotation was measured using a Rudolph Research Analytical AUTOPOL IV digital polarimeter. HRESI MS experiments were obtained using an Agilent 6230 TOF LC-MS.

Collection of *Drifa* sp. samples. The four individuals of *Drifa* sp. were collected by *ROV Holland 1* from the deep sea (54.26007932 N, 11.58046619 W) at a depth of 823 meters during a 2018 cruise of *RV Celtic Explorer* (Cruise CE18012). *In situ* photographs were taken and the specimens are identified as *Drifa* based on gross morphology visible in these. Any epibionts were removed and a small voucher was removed and placed in 96% ethanol. The remainder of the biomass was frozen at -80 °C on board the *RV Celtic Explorer*. The samples were lyophilized upon arrival to National University of Ireland, Galway and stored at -20 °C, then transported to University of South Florida and stored at -20 °C until further processing.

Extraction and Isolation of Natural Products. Upon arrival at the University of South Florida, the specimens were extracted with 100% dichloromethane via reflux (40 °C) with a Soxhlet apparatus. From the 88 g of lyophilized sample, 14.3 g of extract was obtained. A dichloromethane/water partition was performed, resulting in 13.7 g of extract in the organic layer. Initial separation was performed using NP MPLC with a silica column. A linear gradient of hexanes to ethyl acetate over thirty minutes, followed by isocratic 100% ethyl acetate for eight minutes, and then 20% methanol and 80% ethyl acetate for seven minutes. All resulting fractions were dried using passive air or nitrogen. Thirteen fractions were obtained and based on NMR spectroscopic data, the fourth through sixth fractions (eluting roughly around 0% to 35% ethyl acetate) were selected for further purification. Iterations of NP HPLC were performed leading to the isolation of 36.8 mg of tuaimenal A (**1**).

Tuaimenal A (**1**): yellow oil; $[\alpha]^{20}_{D}$ 0.7 (c 0.007, $CHCl_3$); UV (ACN) λ_{max} (log ε): 198 nm (3.2); IR ν (thin film): 2980, 2930, 2880, 1633, 1612, 1483, 1329, 1284 cm^{-1}; ^{1}H and ^{13}C NMR data, Table 1; HRESIMS *m*/z 371.2216 $[M + H]^+$ (calculated for 371.2217, $C_{23}H_{31}O_4$).

Vibrational Circular Dichroism Measurements. Tuaimenal A (**1**) (5.7 mg) was dissolved in 220 µL $CDCl_3$ and transferred to a BaF_2 IR cell with path length of 100 µm. Instrumentation was a BioTools (Jupiter, Florida) ChiralIR 2X DualPEM FT-VCD, resolution 4 cm^{-1}, PEM maximum frequency 1400 cm^{-1}. The sample was measured for 24 blocks of 1 hour each while purged with dry air to remove water vapor. The IR was processed by solvent subtraction and offset to zero at 2000 cm^{-1}. The VCD blocks were averaged, then subtracted using a solvent baseline to produce the final spectrum.

Vibrational Circular Dichroism Calculations. *R*-Tuaimenal A (**1**) was subjected to a GMMX (MMF94) search using BioTools ComputeVOA® software to find the lowest energy conformers in a 5 Kcal/mol range. A total of 805 conformers were minimized using Gaussian 09 at the 631G(d)/B3LYP level with CPCM solvent (chloroform) model. IR and VCD frequencies were calculated at the same level, then duplicates were removed. The 338 lowest energy unique conformers were then Boltzmann averaged and plotted with a line width of 5 cm^{-1}. IR and VCD spectra were then frequency scaled by a factor of 0.968 and compared to the experimental data.

Ligand Preparation. The Tuaimenal A (**1**) structure was prepared for molecular docking studies with Schrödinger's Ligand Preparation Tool (LigPrep).[40] Protonation states of Tuaimenal A were generated using Epik[41] around a target pH of 7.0 +/- 2.0. The structures were able to tautomerize and were desalted before final poses were given. The specified chirality of the molecule was retained. The generated ligands for tuaimenal A were capped at 32 conformations of energetically minimized output structures.

Protein Structure Preparation and Grid Generation. Structures of SARS-CoV-2 protein targets considered in this work were largely collected from the PDB: 3CLpro/Mpro (6LU7),[42] PLpro (6W9C),[43] and RdRp (7BV2).[26] The exception being TMPRSS2, which was built as a homology model using SWISS-MODEL.[44] To relax these protein structures under biologically relevant conditions, structures of 3CLpro, PLpro, RdRp, and TMPRSS2 were solvated and neutralized in water boxes, and then subjected to molecular dynamics simulations according to the following procedures. First, all receptor targets were pre-processed through CHARMMing.org[45] (CHARMM web interface and graphics) to determine amino acid protonation states (via PROPKA),[46] add missing hydrogens, and assign correct bond orders. Each protein was then solvated with 46,656 TIP3 waters in a 90 x 90 x 90 $Å^3$ water box using CHARMM (Chemistry at

HARvard Molecular Mechanics)[47] version C41A1 with C36 protein parameters. The number of counterions needed to achieve a net zero charge for the system was calculated and randomly placed in the water box using a Monte Carlo based method. Next, each system was heated from 110K to 310K using CHARMM molecular dynamics over a 400 ps time scale. To ensure each protein was then sufficiently relaxed, each system was then equilibrated for another 20 ns at 310K. From this equilibrium trajectory, unique conformations of each protein structure were selected by clustering the RMSD of each active site. Active site definitions for each protein can be found in the Supporting Information (Table S1). Using an RMSD threshold of 2 Å, an average of seven unique protein conformations were generated for each SARS-CoV-2 protein target to be used in the docking procedures. As a result of the increased computational time of flexible docking relative to rigid docking, three protein conformations of 3CLpro and PLpro (and two conformations of TMPRSS2 and RdRp) were used as receptors for the flexible docking in this study.

Final protein conformations generated from a flexible docking of antiviral compounds into these prepared protein systems (from another study) were also used as initial target receptors for the rigid docking portion of this current study. These final structures have already adopted favorable conformations to accommodate large antiviral ligands through application of the same flexible ligand/flexible receptor docking protocol used in this work (CIFDock). In total, five "optimized" final protein conformations were used as different initial receptor structures for all protein targets in the rigid docking portion of this study (i.e., tuaimenal A (**1**) was rigidly docked into five different conformers each of 3CLpro, PLpro, TMPRSS2, and RdRp).

Schrödinger's Protein Preparation Wizard[48] was used in convert clustered structures resultant from molecular dynamics simulations in CHARMM to receptor structure files compatible with Schrödinger's Glide Docking.[49] Correct bond orders were assigned, missing hydrogens were

added, disulfide bonds were created, waters beyond five Å from heterogroups were deleted, and protonation states were generated using PropKa for a pH range of 7.0 +/- 2.0. After preprocessing was complete, water orientations were sampled and then optimized. Waters with less than three hydrogen bonds to non-hydrogen atoms were removed from the protein structure. A restrained minimization was then performed in the final processing step, where heavy atoms were converged to an RMSD of 0.30 Å using an OPLS3e force field. The Glide Receptor Grid Generation tool was used to convert complete protein structure files, into minimized receptor structure files represented as simplified interaction grids. For the optimized protease conformations, binding residues were specified, and the centroid of the selected residues served as the center of the binding site. Information on the residue numbers selected in the definition of the active site of each protein target can be found in Supporting Information (Table S1). After selecting the binding site, rotatable groups were visually selected based on proximity to the centroid and with careful consideration of any residue that would have obstructed the active site. Rotatable groups were selected separately for each conformation following these guidelines.

Rigid Docking. Schrödinger's Glide application was used to conduct the initial molecular docking of tuaimenal A (**1**). Ligand conformations were sampled flexibly while the protein receptor remained rigid. The van der Waals radii of the ligand atoms was set to a scaling factor of 0.80 and a partial atomic charge cutoff of 0.15 to soften the potential when considering nonpolar regions of the ligands. The prepared ligands were then computationally bound to the respective targets using extra precision (XP) virtual screening settings.

Flexible Docking. CHARMM-based flexible docking method (CIFDock)[28] was used to flexibly dock (flexible ligand/flexible receptor) tuaimenal A (**1**) into all protein targets (e.g., 3CLpro, PLpro, TMPRSS2, and RdRp). CIFDock incorporates induced fit, in which ligand and

protein conformational degrees of freedom can affect one another during initial approach and complexation. CIFDock thus allows full flexibility of the protein binding site and the ligand, as well as retaining explicit solvent interactions throughout the docking procedure. To achieve this level of flexibility, bulky residues in the active site of a protein that may intrude upon the user-defined binding site when sampled with dynamics were first mutated to alanine. This allows for a more "open" binding site that is better able to accommodate larger and more flexible ligands. Ligand flexibility is achieved by generating conformations using the Confab module of Open Babel.[50] 200 ligand conformations were generated via Confab by rotating any rotatable bonds in the molecule and saving these conformations as unique structure files. Next, these unique ligand conformations were randomly placed in the protein active site and 5 ps of SGLD (Self-Guided Langevin Dynamics)[51] are run on the ligand with a fixed receptor to produce a variety of initial conformations. Finally, those residues which were mutated to alanine in the user-defined binding site are back-mutated to their original residues. Finally, the entire ligand and surrounding protein residues in the binding site (up to 9 Ångstroms outward from any ligand atom) are simulated with two rounds of 2 ps of SGLD (once before explicit waters are added back in, and once after) to allow sampling of the protein-ligand complex conformational space, with possible ligand-induced conformational changes of the active site. A set of custom-designed scoring functions are combined into an ensemble docking score to evaluate the poses generated by CIFDock by analyzing interaction energies (e.g., electrostatic interactions, van der Waals, solvation energies, etc.). The top 20 ranked poses, as determined by the CIFDock scoring functions, were then also given a Glide score by evaluating the poses with Schrödinger's Glide XP scoring function.

Screening SARS-CoV-2 inhibitory properties of Tuaimenal A (1).

Enzymes: The recombinant *F. hepatica* cathepsin L1 (FhCL1) and L3 (FhCL3) zymogens were produced in methanotrophic yeast *Pichia pastoris* and purified as previously described.[52] For the enzymatic assays, the recombinant *F. hepatica* zymogens were activated by mixing each of them with activation buffer (0.1 M sodium citrate buffer, 2 mM DTT, 2.5 mM EDTA, pH 4.5) and incubating for 2 hours (FhCL1) or 3 hours (FhCL3) at 37 °C. The human cathepsin L (HsCL) was activated as described above for 45 min at 37 °C. HsCL, chymotrypsin, trypsin and thrombin were acquired from Sigma-Aldrich.

The SARS-CoV-2 protease, 3CLpro, sequence was codon optimized for expression in *E. coli* cells and synthesized in the pET-28a(+) vector (kanamycin resistant) with a C-terminal His-tag (Genscript). The synthesized vector was transformed into BL21 competent *E. coli* cells (ThermoFisher Scientific), which were cultured in LB broth containing kanamycin (1 μg/mL) at 37 °C. Once an OD600 was reached, protein expression was induced with 1 mM isopropyl-β-D-1-thiogalactopyranoside (IPTG; ThermoFisher Scientific) for 3 hours at 30 °C. Following centrifugation at 10,000 x g for 10 min at 4 °C, the bacteria pellet was digested with lysozyme (10 μg/mL) and sonicated. Subsequent centrifugation at 10,000 x g for 10 min at 4 °C was used to recover the soluble recombinant 3CLpro within the supernatant that was purified using the Profinia Affinity Chromatography Protein Purification System (Bio-Rad), with the mini profinity IMAC and mini Bio-Gel P− 6 desalting cartridges (Bio-Rad).

Assay conditions: Unless otherwise stated, all enzymes were assayed in a 100 μL reaction volume using appropriate buffer (Table 3) for each enzyme. Enzymatic concentration and substrates used in the screening assays are presented in Table 3. Initially, the reaction buffer was mixed with 20 μM tuaimenal A (**1**) (for IC_{50} experiments serial dilutions from 20 μM were used) and the enzyme was then added to the reaction and incubated for 15 min at 37 °C before the fluorogenic substrate

was added. The broad-spectrum inhibitors E-64 (100 μM; Sigma-Aldrich) or AEBSF (5 mM; Sigma-Aldrich) were used as a positive control inhibitor of cysteine and serine proteases, respectively. Hydrolytic activity was measured over 1 hour, at 37 °C as relative fluorescent units (RFU) in a PolarStar Omega Spectrophotometer (BMG LabTech). All assays were carried out in triplicate and the results were analyzed using GraphPad Prism 5.0 Software.

Table 3. Assay conditions for each enzyme screened with tuaimenal A (**1**).

Enzyme (concentration)	Buffer	Substrate
HsCL (0.2 nM)	Sodium acetate[A]	Z-Phe-Arg-NHMec (20 μM)
Bovine α-Chymotrypsin (4 nM)	Tris HCl[B]	Suc-Ala-Ala-Pro-Phe-NHMec (20 μM)
Bovine Trypsin (168 nM)	Tris HCl	Z-Leu-Arg-NHMec (20 μM)
Bovine Thrombin (800 pM)	Tris HCl	Z-Gly-Pro-Arg-NHMec (20 μM)
3CLpro (500 nM)	Hepes Buffer[C]	LGSAVLQ-rhodamine 110-dp (20 μM)
FhCL1 (2.7 nM)	Tris HCl	Z-Leu-Arg-NHMec (20 μM)
FhCL3 (5 nM)	Sodium acetate	Z-Gly-Pro-Arg-NHMec (20 μM)

A: 100 nM Sodium acetate, 1 mM EDTA, 1 mM DTT, 0.01% Brij L23, pH 5,5.
B: 50 mM TRIS, 100 mM NaCl, 1 mM EDTA, pH 7,0.
C: 20 mM Hepes, 2 mM EDTA, pH 7,4.

The fluorogenic substrates were acquired from Bachem or BostonBiochem (LGSAVLQ-rhodamine 110-dp).

Bioassay Using Cervical Cancer Cell Lines. The cervical cancer cells line, CaSki, and C33A, were cultured in RPMI 1640 and DMEM complete media, respectively, supplemented with 10% Fetal Bovine Serum (FBS), 100 units/ mL of penicillin, 100 mg/mL of streptomycin, 2 mM L-glutamines, 1 mM sodium pyruvate, NEAA 0.1mM, 0.05 mM 2-mercaptoethanol, 0.5 mg/mL amphotericin B and 0.5 mg/mL gentamycin. CaSki (ATCC, CRM-CRL-1550) and C33A (ATCC, HTB-31) were kept at passages less than 10, mycoplasma tested quarterly and maintained in an incubator at 37 °C and 5% CO_2 atmosphere. Cells were seeded in to 96-well plate at 1,000 cells per well with 200 μL of media. The cells were treated with 1% dimethyl sulfoxide (DMSO Control,

N=6) and different concentrations of tuaimenal A (**1**) (10 µM, 1 µM, 0.1 µM and 0.01 µM, *N*=6). After 24 hours post treatment, the cell proliferation was assessed using Water-Soluble Tetrazolium (WST-1, Roche, 5015944001). The plates were read on a BioTek SynergyHT microplate reader, at wavelengths 450 and 600 nm (with the 450 nm signal corrected by subtracting the 600 nm signal). Statistical analysis for tuaimenal A (**1**) effects of CaSki and C33A cells proliferation was processed in GraphPad Prism using a one-way ANOVA with a Tukey's multiple comparisons test.

ASSOCIATED CONTENT

The following Supporting Information is available:

^{1}H, ^{13}C, 2D NMR, HRESIMS, UV, FTIR spectra, and VCD data for tuaimenal A (**1**);

binding site residues for rigid docking with 3CLpro, Plpro, RdRp, and TMPRSS2 protein targets (PDF).

AUTHOR INFORMATION

Corresponding Authors

A. Louise Allcock, Department of Zoology, National University of Ireland Galway, Galway, Ireland; Email: louise.allcock@nuigalway.ie

Baker, Bill J., University of South Florida, Department of Chemistry, 4202 E. Fowler Ave. CHE205, Tampa, FL 33620; bjbaker@usf.edu

Present Addresses

[†]Nicole E. Avalon, Center for Marine Biotechnology and Biomedicine, Scripps Institution of Oceanography, University of California San Diego, La Jolla, California 92093, United States

[†]Fiona L. Kearns, University of California San Diego, Department of Chemistry and Biochemistry, La Jolla, California 92093, United States

ORCiDs for Authors

Nicole E. Avalon	0000-0003-3588-892X
Jordan Nafie	0000-0003-1986-0302
Tracess Smalley	0000-0002-3295-7443
Carolina de Marco Verissimo	0000-0003-1762-6387
Sarah G. Dietrick	0000-0002-1566-1958
Ryan M. Young	0000-0002-5340-6827
Luke C. Warrensford	0000-0002-9206-5121
Amanda R. Pittman	0000-0002-5820-2268
Fiona L. Kearns	0000-0002-5469-9035
Jennifer M. Binning	0000-0001-5871-686X
John P. Dalton	0000-0003-3829-9186
Mark P. Johnson	0000-0002-5078-1410
H. Lee Woodcock	0000-0003-3539-273X
A. Louise Allcock	0000-0002-4806-0040
Bill J. Baker	0000-0003-3033-5779

Author Contributions

The manuscript was written through contributions of all authors. All authors have given approval to the final version of the manuscript.

This work was the result of a team effort in which the following contributions are recognized: methodology and experimentation, N.E.A., J.N., T.S., J.M.B., C.M.V., J.P.D., S.G.D., L.C.W., A.R.P., F.L.K., H.L.W, B.J.B; data analysis, N.E.A., J.N., T.S., C.M.V., J.P.D., S.G.D., L.C.W., A.R.P., F.L.K., R.M.Y, B.J.B.; original draft preparation, N.E.A., B.J.B., J.N., T.S., J.M.B., C.M.V., J.P.D., S.G.D., L.C.W., A.R.P.; review and editing, N.E.A., B.J.B., A.L.A., J.N., T.S., J.M.B., C.M.V., J.P.D., S.G.D., L.C.W., A.R.P., F.L.K., R.M.Y., M.P.J, H.L.W.; funding acquisition, B.J.B., A.L.A., and J.P.D.

ACKNOWLEDGMENTS

This publication has emanated from research supported by a research grant from Science Foundation Ireland (SFI) and the Marine Institute under the Investigators Programme Grant No. SFI/15/1A/3100, co-funded under the European Regional Development Fund 2014-2020 to A.L.A., and also the project NMBLI (Grant-Aid Agreement PBA/MB/16/01). Research at USF was supported NIH Grant R56 AI154922 (to B.J.B. and Dr. L.N. Shaw). Portions of this work were also supported by the Science Foundation Ireland (SFI) COVID-19 Rapid Response Funding Call, proposal ID 20/COV/0023 (to J.P.D). Subsea photographs taken by NUI Galway, copyright Marine Institute, during cruise CE18012 funded under SFI/15/1A/3100. We gratefully acknowledge the assistance of the science party and crew of the *RV Celtic Explorer* and the pilots of the *ROV Holland I*, without whose distinctive expertise this research would not be possible. S.

Afoullouss is acknowledged for his assistance with sample collection and initial processing. The students G. Shaw, S. Suarez, and M. Silas are recognized for their technical assistance with this project. We also recognize the assistance of Dr L. Calcul and J. Welsch with the Chemical Purification, Analysis, and Screening Facility at USF.

REFERENCES

(1) Roberts, J. M.; Wheeler, A.; Freiwald, A.; Cairns, S. *Cold-Water Corals: The Biology and Geology of Deep-Sea Coral Habitats*; Cambridge University Press, 2009.

(2) Skropeta, D.; Wei, L. Recent Advances in Deep-Sea Natural Products. *Nat. Prod. Rep.* **2014**, *31* (8), 999–1025. https://doi.org/10.1039/C3NP70118B.

(3) Carroll, A. R.; Copp, B. R.; Davis, R. A.; Keyzers, R. A.; Prinsep, M. R. Marine Natural Products. *Nat. Prod. Rep.* **2021**, *38* (2), 362–413. https://doi.org/10.1039/D0NP00089B.

(4) Daly, M.; Brugler, M. R.; Cartwright, P.; Collins, A. G.; Dawson, M. N.; Fautin, D. G.; France, S. C.; McFadden, C. S.; Opresko, D. M.; Rodriguez, E.; Romano, S. L.; Stake, J. L. The Phylum Cnidaria: A Review of Phylogenetic Patterns and Diversity 300 Years after Linnaeus*. *Zootaxa* **2007**, *1668* (1), 127–182. https://doi.org/10.11646/zootaxa.1668.1.11.

(5) Hu, J.; Yang, B.; Lin, X.; Zhou, X.; Yang, X.; Long, L.; Liu, Y. Chemical and Biological Studies of Soft Corals of the Nephtheidae Family. *Chem. Biodivers.* **2011**, *8* (6), 1011–1032. https://doi.org/10.1002/cbdv.201000105.

(6) Cucinotta, D.; Vanelli, M. WHO Declares COVID-19 a Pandemic. *Acta Biomed. Atenei Parm.* **2020**, *91* (1), 157–160. https://doi.org/10.23750/abm.v91i1.9397.

(7) Dong, E.; Du, H.; Gardner, L. An Interactive Web-Based Dashboard to Track COVID-19 in Real Time. *Lancet Infect. Dis.* **2020**, *20* (5), 533–534. https://doi.org/10.1016/S1473-

3099(20)30120-1.

(8) Ferlay, J.; Ervik, M.; Lam, F.; Colombet, M.; Mery, L.; Piñeros, M.; Znaor, A.; Soerjomataram, I.; Bray, F. Global Cancer Observatory: Cancer Today https://gco.iarc.fr/today (accessed 2022-01-11).

(9) Sung, H.; Ferlay, J.; Siegel, R. L.; Laversanne, M.; Soerjomataram, I.; Jemal, A.; Bray, F. Global Cancer Statistics 2020: GLOBOCAN Estimates of Incidence and Mortality Worldwide for 36 Cancers in 185 Countries. *CA. Cancer J. Clin.* **2021**, *71* (3), 209–249. https://doi.org/10.3322/caac.21660.

(10) Huang, M.; Lu, J.-J.; Ding, J. Natural Products in Cancer Therapy: Past, Present and Future. *Nat. Products Bioprospect.* **2021**, *11* (1), 5–13. https://doi.org/10.1007/s13659-020-00293-7.

(11) Demain, A. L.; Vaishnav, P. Natural Products for Cancer Chemotherapy. *Microb. Biotechnol.* **2011**, *4* (6), 687–699. https://doi.org/10.1111/j.1751-7915.2010.00221.x.

(12) Beigel, J. H.; Tomashek, K. M.; Dodd, L. E.; Mehta, A. K.; Zingman, B. S.; Kalil, A. C.; Hohmann, E.; Chu, H. Y.; Luetkemeyer, A.; Kline, S.; Lopez de Castilla, D.; Finberg, R. W.; Dierberg, K.; Tapson, V.; Hsieh, L.; Patterson, T. F.; Paredes, R.; Sweeney, D. A.; Short, W. R.; Touloumi, G.; Lye, D. C.; Ohmagari, N.; Oh, M.; Ruiz-Palacios, G. M.; Benfield, T.; Fätkenheuer, G.; Kortepeter, M. G.; Atmar, R. L.; Creech, C. B.; Lundgren, J.; Babiker, A. G.; Pett, S.; Neaton, J. D.; Burgess, T. H.; Bonnett, T.; Green, M.; Makowski, M.; Osinusi, A.; Nayak, S.; Lane, H. C. Remdesivir for the Treatment of Covid-19 — Final Report. *N. Engl. J. Med.* **2020**, *383* (19), 1813–1826. https://doi.org/10.1056/NEJMoa2007764.

(13) Zhai, P.; Ding, Y.; Wu, X.; Long, J.; Zhong, Y.; Li, Y. The Epidemiology, Diagnosis and

Treatment of COVID-19. *Int. J. Antimicrob. Agents* **2020**, *55* (5), 105955. https://doi.org/10.1016/j.ijantimicag.2020.105955.

(14) Tuaimenal (pronounced twam-ene-al) is derived from tuaimneacha, the Irish Gaelic word used to describe the sound of waves crashing against the rocks.

(15) He, Y.; Bo, W.; Dukor, R. K.; Nafie, L. A. Determination of Absolute Configuration of Chiral Molecules Using Vibrational Optical Activity: A Review. *Appl. Spectrosc.* **2011**, *65* (7), 699–723. https://doi.org/10.1366/11-06321.

(16) Merten, C.; Golub, T. P.; Kreienborg, N. M. Absolute Configurations of Synthetic Molecular Scaffolds from Vibrational CD Spectroscopy. *J. Org. Chem.* **2019**, *84* (14), 8797–8814. https://doi.org/10.1021/acs.joc.9b00466.

(17) Polavarapu, P. L.; Santoro, E. Vibrational Optical Activity for Structural Characterization of Natural Products. *Nat. Prod. Rep.* **2020**, *37* (12), 1661–1699. https://doi.org/10.1039/D0NP00025F.

(18) Chamberlain, B. T.; Vincent, M.; Nafie, J.; Müller, P.; Greka, A.; Wagner, F. F. Multigram Preparation of BRD4780 Enantiomers and Assignment of Absolute Stereochemistry. *J. Org. Chem.* **2021**, *86* (5), 4281–4289. https://doi.org/10.1021/acs.joc.0c02520.

(19) Devlin, F. J.; Stephens, P. J.; Cheeseman, J. R.; Frisch, M. J. Ab Initio Prediction of Vibrational Absorption and Circular Dichroism Spectra of Chiral Natural Products Using Density Functional Theory: α-Pinene. *J. Phys. Chem. A* **1997**, *101* (51), 9912–9924. https://doi.org/10.1021/jp971905a.

(20) Polavarapu, P. L.; Covington, C. L. Comparison of Experimental and Calculated Chiroptical Spectra for Chiral Molecular Structure Determination. *Chirality* **2014**, *26* (9),

539–552. https://doi.org/10.1002/chir.22316.

(21) Debie, E.; De Gussem, E.; Dukor, R. K.; Herrebout, W.; Nafie, L. A.; Bultinck, P. A Confidence Level Algorithm for the Determination of Absolute Configuration Using Vibrational Circular Dichroism or Raman Optical Activity. *ChemPhysChem* **2011**, *12* (8), 1542–1549. https://doi.org/10.1002/cphc.201100050.

(22) Luan, B.; Huynh, T.; Cheng, X.; Lan, G.; Wang, H.-R. Targeting Proteases for Treating COVID-19. *J. Proteome Res.* **2020**, *19* (11), 4316–4326. https://doi.org/10.1021/acs.jproteome.0c00430.

(23) Anand, K.; Ziebuhr, J.; Wadhwani, P.; Mesters, J. R.; Hilgenfeld, R. Coronavirus Main Proteinase (3CL pro) Structure: Basis for Design of Anti-SARS Drugs. *Science (80-.).* **2003**, *300* (5626), 1763–1767. https://doi.org/10.1126/science.1085658.

(24) Zhang, L.; Lin, D.; Sun, X.; Curth, U.; Drosten, C.; Sauerhering, L.; Becker, S.; Rox, K.; Hilgenfeld, R. Crystal Structure of SARS-CoV-2 Main Protease Provides a Basis for Design of Improved α-Ketoamide Inhibitors. *Science (80-.).* **2020**, *368* (6489), 409–412. https://doi.org/10.1126/science.abb3405.

(25) Hoffmann, M.; Kleine-Weber, H.; Schroeder, S.; Krüger, N.; Herrler, T.; Erichsen, S.; Schiergens, T. S.; Herrler, G.; Wu, N.-H.; Nitsche, A.; Müller, M. A.; Drosten, C.; Pöhlmann, S. SARS-CoV-2 Cell Entry Depends on ACE2 and TMPRSS2 and Is Blocked by a Clinically Proven Protease Inhibitor. *Cell* **2020**, *181* (2), 271-280.e8. https://doi.org/10.1016/j.cell.2020.02.052.

(26) Yin, W.; Luan, X.; Li, Z.; Zhou, Z.; Wang, Q.; Gao, M.; Wang, X.; Zhou, F.; Shi, J.; You, E.; Liu, M.; Wang, Q.; Jiang, Y.; Jiang, H.; Xiao, G.; Zhang, L.; Yu, X.; Zhang, S.; Eric Xu, H. Structural Basis for Inhibition of the SARS-CoV-2 RNA Polymerase by Suramin.

Nat. Struct. Mol. Biol. **2021**, *28* (3), 319–325. https://doi.org/10.1038/s41594-021-00570-0.

(27) Friesner, R. A.; Murphy, R. B.; Repasky, M. P.; Frye, L. L.; Greenwood, J. R.; Halgren, T. A.; Sanschagrin, P. C.; Mainz, D. T. Extra Precision Glide: Docking and Scoring Incorporating a Model of Hydrophobic Enclosure for Protein−Ligand Complexes. *J. Med. Chem.* **2006**, *49* (21), 6177–6196. https://doi.org/10.1021/jm051256o.

(28) Vankayala, S. L.; Warrensford, L. C.; Pittman, A. R.; Pollard, B. C.; Kearns, F. L.; Larkin, J. D.; Woodcock, H. L. CIFDock: A Novel CHARMM-based Flexible Receptor–Flexible Ligand Docking Protocol. *J. Comput. Chem.* **2022**, *43* (2), 84–95. https://doi.org/10.1002/jcc.26759.

(29) Colunga Biancatelli, R. M. L.; Berrill, M.; Catravas, J. D.; Marik, P. E. Quercetin and Vitamin C: An Experimental, Synergistic Therapy for the Prevention and Treatment of SARS-CoV-2 Related Disease (COVID-19). *Front. Immunol.* **2020**, *11* (June), 1–11. https://doi.org/10.3389/fimmu.2020.01451.

(30) Hariono, M.; Hariyono, P.; Dwiastuti, R.; Setyani, W.; Yusuf, M.; Salin, N.; Wahab, H. Potential SARS-CoV-2 3CLpro Inhibitors from Chromene, Flavonoid and Hydroxamic Acid Compound Based on FRET Assay, Docking and Pharmacophore Studies. *Results Chem.* **2021**, *3* (January), 100195. https://doi.org/10.1016/j.rechem.2021.100195.

(31) Dr. Roli, J.; Dr. Sandeep, S.; Dr. Neeti, N.; Dr. Archna, P. A Systemic Review: Structural Mechanism of SARS-CoV-2A Promising Preventive Cure by Phytochemicals. *Int. J. Immunol. Immunother.* **2020**, *7* (2), 1–8. https://doi.org/10.23937/2378-3672/1410051.

(32) Chen, C.-N.; Lin, C. P. C.; Huang, K.-K.; Chen, W.-C.; Hsieh, H.-P.; Liang, P.-H.; Hsu, J. T. A. Inhibition of SARS-CoV 3C-like Protease Activity by Theaflavin-3,3'-Digallate

(TF3). *Evidence-Based Complement. Altern. Med.* **2005**, *2* (2), 209–215. https://doi.org/10.1093/ecam/neh081.

(33) de Vries, M.; Mohamed, A. S.; Prescott, R. A.; Valero-Jimenez, A. M.; Desvignes, L.; O'Connor, R.; Steppan, C.; Devlin, J. C.; Ivanova, E.; Herrera, A.; Schinlever, A.; Loose, P.; Ruggles, K.; Koralov, S. B.; Anderson, A. S.; Binder, J.; Dittmann, M. A Comparative Analysis of SARS-CoV-2 Antivirals Characterizes 3CL pro Inhibitor PF-00835231 as a Potential New Treatment for COVID-19. *J. Virol.* **2021**, *95* (10). https://doi.org/10.1128/JVI.01819-20.

(34) Ghosh, R.; Chakraborty, A.; Biswas, A.; Chowdhuri, S. Identification of Alkaloids from Justicia Adhatoda as Potent SARS CoV-2 Main Protease Inhibitors: An in Silico Perspective. *J. Mol. Struct.* **2021**, *1229*, 129489. https://doi.org/10.1016/j.molstruc.2020.129489.

(35) Mahase, E. Covid-19: Pfizer's Paxlovid Is 89% Effective in Patients at Risk of Serious Illness, Company Reports. *BMJ* **2021**, *375*, n2713. https://doi.org/10.1136/bmj.n2713.

(36) Parums, D. V. Editorial: Current Status of Oral Antiviral Drug Treatments for SARS-CoV-2 Infection in Non-Hospitalized Patients. *Med. Sci. Monit.* **2022**, *28*. https://doi.org/10.12659/MSM.935952.

(37) Cragg, G. M.; Pezzuto, J. M. Natural Products as a Vital Source for the Discovery of Cancer Chemotherapeutic and Chemopreventive Agents. *Med. Princ. Pract.* **2016**, *25* (2), 41–59. https://doi.org/10.1159/000443404.

(38) Park, S.-H.; Kim, M.; Lee, S.; Jung, W.; Kim, B. Therapeutic Potential of Natural Products in Treatment of Cervical Cancer: A Review. *Nutrients* **2021**, *13* (1), 154. https://doi.org/10.3390/nu13010154.

(39) Eatemadi, A.; Aiyelabegan, H. T.; Negahdari, B.; Mazlomi, M. A.; Daraee, H.; Daraee, N.; Eatemadi, R.; Sadroddiny, E. Role of Protease and Protease Inhibitors in Cancer Pathogenesis and Treatment. *Biomed. Pharmacother.* **2017**, *86*, 221–231. https://doi.org/10.1016/j.biopha.2016.12.021.

(40) LigPrep, Schrödinger, LLC, New York, NY, 2021.

(41) Shelley, J. C.; Cholleti, A.; Frye, L. L.; Greenwood, J. R.; Timlin, M. R.; Uchimaya, M. Epik: A Software Program for PK a Prediction and Protonation State Generation for Drug-like Molecules. *J. Comput. Aided. Mol. Des.* **2007**, *21* (12), 681–691. https://doi.org/10.1007/s10822-007-9133-z.

(42) Jin, Z.; Du, X.; Xu, Y.; Deng, Y.; Liu, M.; Zhao, Y.; Zhang, B.; Li, X.; Zhang, L.; Peng, C.; Duan, Y.; Yu, J.; Wang, L.; Yang, K.; Liu, F.; Jiang, R.; Yang, X.; You, T.; Liu, X.; Yang, X.; Bai, F.; Liu, H.; Liu, X.; Guddat, L. W.; Xu, W.; Xiao, G.; Qin, C.; Shi, Z.; Jiang, H.; Rao, Z.; Yang, H. Structure of Mpro from SARS-CoV-2 and Discovery of Its Inhibitors. *Nature* **2020**, *582* (7811), 289–293. https://doi.org/10.1038/s41586-020-2223-y.

(43) Osipiuk, J., Jedrzejczak, R., Tesar, C., Endres, M., Stols, L., Babnigg, G., Kim, Y., Michalska, K., Joachimiak, A., C. for S. G. of I. D. (CSGID). The Crystal Structure of Papain-like Protease of SARS CoV-2. *PDB* **2020**. https://doi.org/10.2210/pdb6w9c/pdb.

(44) Schwede, T. SWISS-MODEL: An Automated Protein Homology-Modeling Server. *Nucleic Acids Res.* **2003**, *31* (13), 3381–3385. https://doi.org/10.1093/nar/gkg520.

(45) Miller, B. T.; Singh, R. P.; Klauda, J. B.; Hodošček, M.; Brooks, B. R.; Woodcock, H. L. CHARMMing: A New, Flexible Web Portal for CHARMM. *J. Chem. Inf. Model.* **2008**, *48* (9), 1920–1929. https://doi.org/10.1021/ci800133b.

(46) Bas, D. C.; Rogers, D. M.; Jensen, J. H. Very Fast Prediction and Rationalization of PKa Values for Protein-Ligand Complexes. *Proteins Struct. Funct. Bioinforma.* **2008**, *73* (3), 765–783. https://doi.org/10.1002/prot.22102.

(47) Vanommeslaeghe, K.; Hatcher, E.; Acharya, C.; Kundu, S.; Zhong, S.; Shim, J.; Darian, E.; Guvench, O.; Lopes, P.; Vorobyov, I.; Mackerell, A. D. CHARMM General Force Field: A Force Field for Drug-like Molecules Compatible with the CHARMM All-Atom Additive Biological Force Fields. *J. Comput. Chem.* **2009**, NA-NA. https://doi.org/10.1002/jcc.21367.

(48) Protein Preparation Wizard; Epik, Schrödinger, LLC, New York, NY, 2021; Impact, Schrödinger, LLC, New York, NY; Prime, Schrödinger, LLC, New York, NY, 2021.

(49) Friesner, R. A.; Banks, J. L.; Murphy, R. B.; Halgren, T. A.; Klicic, J. J.; Mainz, D. T.; Repasky, M. P.; Knoll, E. H.; Shelley, M.; Perry, J. K.; Shaw, D. E.; Francis, P.; Shenkin, P. S. Glide: A New Approach for Rapid, Accurate Docking and Scoring. 1. Method and Assessment of Docking Accuracy. *J. Med. Chem.* **2004**, *47* (7), 1739–1749. https://doi.org/10.1021/jm0306430.

(50) O'Boyle, N. M.; Banck, M.; James, C. A.; Morley, C.; Vandermeersch, T.; Hutchison, G. R. Open Babel: An Open Chemical Toolbox. *J. Cheminform.* **2011**, *3* (1), 33. https://doi.org/10.1186/1758-2946-3-33.

(51) Wu, X.; Brooks, B. R. Self-Guided Langevin Dynamics Simulation Method. *Chem. Phys. Lett.* **2003**, *381* (3–4), 512–518. https://doi.org/10.1016/j.cplett.2003.10.013.

(52) Robinson, M. W.; Corvo, I.; Jones, P. M.; George, A. M.; Padula, M. P.; To, J.; Cancela, M.; Rinaldi, G.; Tort, J. F.; Roche, L.; Dalton, J. P. Collagenolytic Activities of the Major Secreted Cathepsin L Peptidases Involved in the Virulence of the Helminth Pathogen,

Fasciola Hepatica. *PLoS Negl. Trop. Dis.* **2011**, *5* (4), e1012.

https://doi.org/10.1371/journal.pntd.0001012.